Endothelial Slit2 guides the Robo1-positive sympathetic innervation during heart development

Juanjuan Zhao[1], PhD; Susann Bruche[1,2], PhD; Konstantinos Lekkos[1,2], MSc; Carolyn Carr[1], PhD; Joaquim M. Vieira[3], PhD; John G. Parnavelas[4], PhD; William D. Andrews[4], PhD; Mathilda T.M. Mommersteeg, PhD[1,2] ✉

[1] Department of Physiology, Anatomy & Genetics, University of Oxford, Oxford, UK
[2] Institute of Developmental and Regenerative Medicine, Old Road Campus, University of Oxford, Oxford, UK
[3] School of Cardiovascular & Metabolic Medicine & Sciences, Faculty of Life Sciences & Medicine, Kings College London, British Heart Foundation Centre – James Black Centre, London, UK.
[4] Department of Cell and Developmental Biology, University College London, London, UK.

Short title: Slit-Robo signalling in cardiac innervation development

✉ Corresponding author:

Mathilda T.M. Mommersteeg

Institute of Developmental and Regenerative Medicine

Department of Physiology, Anatomy and Genetics

University of Oxford

Old Road Campus, Roosevelt Drive

Oxford OX3 7TY

United Kingdom

Word count: 1481

Abstract

Axon guidance cues direct nerves in the heart during development, disease and regeneration. These cues determine cardiac innervation patterning by regulating the balance between chemo-attraction and chemo-repulsion. However, the role of one of the most crucial ligand-receptor combinations among axon guidance molecules, the Slit chemo-active ligands and their Roundabout (Robo) transmembrane receptors, remains unknown during cardiac innervation patterning. To test if Slit-Robo signalling is important for cardiac innervation guidance, we analysed Slit and Robo mouse knock-outs. Constitutive *Slit2*$^{-/-}$ ventricles showed significantly reduced innervation, while *Slit3*$^{-/-}$ hearts showed temporary increased levels of innervation compared to wild-type littermate controls. Whereas innervation was not affected in *Robo2*$^{-/-}$mice, the phenotype seen in *Slit2*$^{-/-}$ ventricles was recapitulated in *Robo1*$^{-/-}$ mice. Detailed expression analysis identified expression of Slit2 ligand in the endothelium of the coronary vessels, while Slit3 was highly present in the coronary smooth muscle wall and in the innervation. Both the Robo1 and Robo2 receptors were present in the nerves and at low levels in the vessels. Knocking out *Slit2* specifically in the endothelium recapitulated the defects seen in the constitutive *Slit2*$^{-/-}$ hearts. *Ex vivo* axon guidance cultures showed that attraction of axons extending from the ganglia was strongly reduced in ventricles with absence of endothelial Slit2 compared to wild-type controls. In absence of endothelial Slit2, adult mice showed reduced response to challenging the sympathetic innervation. In conclusion, we have identified an important new chemo-active Slit2-Robo1 pathway required for correct cardiac innervation development.

Introduction

A number of recent studies have revealed the extent and importance of the innervation of the heart during disease, regeneration and aging. [1–5] Alterations in the innervation play a role in the susceptibility to arrhythmias in various cardiac diseases, from cardiac ganglia in the pathogenesis of atrial fibrillation, to ventricular nerves in the predilection toward ventricular arrhythmias and sudden cardiac death in myocardial scar areas, chronic congestive heart failure, diabetic neuropathy and diseases such as Long QT and Brugada syndrome.[2,6–11]

Previous studies have shown that neurogenic genes including Semaphorin3a (Sema3a) and its receptor Neuropilin1 (Nrp1), Nerve Growth Factor (NGF), glial cell line-derived neurotrophic factor (GDNF), Edn1 and its receptor Ednra as well as Plexin A4 are involved in determining cardiac innervation patterning during development by regulating the balance between chemo-attraction and chemo-repulsion.[12–18] Some of these pathways are re-activated during aging as accumulation of senescent cells stimulates the release of Sema3a from the coronary vasculature, reducing innervation density in the heart. Tipping the balance towards chemo-repulsive Sema3a and inducing denervation increases the risk of arrhythmias in the aging heart, which is reversible with senolytic drugs.[5] This shows that even after birth, maintaining the balance between chemo-attraction and repulsion remains important throughout life and targetable with therapeutics.

Only a relatively small number of attractive or repulsive axon guidance cues are known and while we now know the involvement of key guidance factors in the heart, knowledge on one major player is still lacking. Here, we report a crucial novel role for the Slit-Robo signalling pathway in cardiac innervation guidance during development. The Roundabout (Robo) transmembrane receptors and their Slit ligands were first studied for their role in axonal guidance in the embryonic nervous system.[19] However, many new roles have been identified since, especially in cancer and embryogenesis.[19,20] In the mammalian heart,

the pathway is involved in cardiac chamber formation, cardiac neural crest migration and adhesion, the development of the pericardium and caval veins, membranous ventricular septum and valve formation.[21–24] Here, using constitutive and conditional knock-out approaches, axon guidance experiments and functional analysis, we show that interaction of Slit2 and Robo1 is important for correct innervation patterning during heart development. This knowledge will help us better understand the mechanisms underling dysregulation of innervation during development, aging and disese and how to promote appropriate nerve growth.

Methods and Data Availability

Mouse lines

All experiments were performed in accordance with the UK Animals (Scientific Procedures) Act 1986 and institutional guidelines. *Robo1*^{tm1Wia} [25] and *Robo2*^{tm1Rilm} [26] were obtained from William Andrews (UCL, London, UK). *Robo1*^{tm1Matl}*;Robo2*^{tm1Rilm},[27] Slit1^{tm1Matl} and Slit2^{tm1Matl},[28] *Slit2*$^{tm1.1Ics}$ [29] from Alain Chedotal (Institut de la Vision, Paris, France). Slit3$^{tm1.1Dor}$ [30] from David Ornitz. [20]*Tg(Wnt1-cre)*^{11Rth},[31] *Tg(Tek-cre)*^{12Flv} (*Tie2-cre*)[32] and *Tg(Myh6-cre/Esr1*)*^{1Jmk} [33] were obtained from the Jackson lab. All lines were maintained on a C57/BL6J background (C57BL/6JOlaHsd, model code 057, Envigo). The day the vaginal plug was found was considered as embryonic day (E) 0.5. Cre allele *Tg(Myh6-cre/Esr1*)*^{1Jmk} was induced by oral gavage with five consecutive doses of 20mg/kg 4-hydroxytamoxifen (Sigma, T5648) at E12.5 to E16.5.

Tissue processing and immunohistochemistry-paraffin section staining

Fluorescent immunohistochemistry was performed as previously described.[34] Embryos were dissected and fixed overnight in 4% paraformaldehyde (ChemCruz, SC-281692). Following a brief wash in PBS (Gibco, 18912-014), the samples were dehydrated using an ethanol gradient (two-hour incubations in 70%, 80%, 90% and 96% and two 1-hour incubations in 100% ethanol, Sigma-Aldrich, 32221-2.5L-M)) before being incubated in 1-butanol (MP biomedicals, 194001) at room temperature overnight. Before mounting the embryos in sectioning moulds, three two-hour incubations were performed in paraffin (Paraplast plus, Sigma-Aldrich, P3683) at 65°C. Using a Leica microtome (Microm HM325), 10μm sections were collected, mounted on Superfrost Plus glass slides (VWR, 631-0108) ensuring even

coverage of the heart (one in every three sections per staining combination) and were allowed to dry overnight at 33°C.

The slides were de-waxed in Xylene (Fisher Scientific, X/0200/17) twice for 5 min and rehydrated in an ethanol gradient (100%, 100%, 96%, 90%, 80%, 70%) for one minute each before being incubated for one more minute in PBS. The samples were then boiled for 4 min in a pressure cooker in antigen unmasking solution (H-3300, Vector Laboratories) and were allowed to cool down in PBS-T (Tween-20 0.1%, Chemcruz, sc-29113) before a ring was drawn around them using an ImmEdge pen (Vector Laboratories, H4000). The sections were blocked for 30 min at room temperature in a humidified chamber using blocking reagent [0.5% blocking reagent powder (Akoya Bioscience, FP1012), 0.15 M NaCl, 0.1 M Tris-HCl (pH 7.5)] and were then incubated with primary antibody diluted blocking solution overnight at room temperature. Following three 5min washes in PBS-T, the secondary antibody was applied (1:200 in blocking solution, Invitrogen, Alexa range) for 2 hours at room temperature.

For the Slit and Robo antibodies, an additional amplification step was added to enhance the signal using the TSA kit (NEL756001KT, Perkin and Elmer). Instead of an Alexa secondary antibody, a biotinylated secondary antibody was used at a 1:200 dilution in blocking solution for 45 min at room temperature, followed by three 5 min washes in PBS-T prior to a 30 min incubation with conjugated Streptavidin-Horse Radish Peroxidase (Vector Laboratories, SA-5004) and then three 5 min washes in PBS-T. Either fluorescein or tetramethylrhodamine (in DMSO, NEL756001KT) diluted at 1:100 in amplification buffer was then added to the sections for 3 min, followed by three 5 min washes with PBS and staining with DAPI (2.5 µg/ml, Sigma, MBD0015). Mowiol 4-88 (Applichem, A9011,1000) was used to mount the slides, which were cured at 37°C in the dark. Primary antibodies against the following proteins were used: goat polyclonal anti-cardiac Troponin I (cTnI,

1:200; Hytest Ltd, 4T21/2), mouse monoclonal anti-Myosin heavy chain (MF20, 1:50, HSHB, AB-2147781), rabbit polyclonal anti-Peripherin (Prph, 1:200; Millipore, AB1530), rabbit polyclonal anti-Tyrosine Hydroxylase (TH, 1:200; Millipore, AB152), goat polyclonal anti-Robo1 (1:200; R&D Systems, AF1749), goat polyclonal anti-Robo2 (1:200; R&D Systems, AF3147), sheep polyclonal anti-Slit2 (1:200; R&D Systems, AF5444), rat monoclonal anti-Slit3 (1:200; R&D Systems, MAB3629), rabbit polyclonal anti-Erg1 (1:200, Abcam, ab110639) and rabbit polyclonal anti-Smooth muscle myosin heavy chain 11 (Myh11, 1:200, Abcam, ab125884). Imaging was performed on a Nikon microscope (Nikon, Eclipse Ci-L). Images were processed using ImageJ to generate magenta and green colour combinations.[35]

Volume measurements

To quantitate the nerve density in the ventricle, every third transverse 10 µm section capturing the entire diameter of the heart was stained as detailed above for cTnI and Peripherin or TH and imaged using a Nikon microscope (Nikon, Eclipse Ci-L). The images were loaded into 3D reconstruction software (Amira 6.3.0, Thermo Fisher Scientific). Images were resampled, aligned and different labels were created for the myocardium of the ventricle based on cTnI thresholding and for the innervation surrounding the ventricle, based on Peripherin thresholding for total innervation or based on TH thresholding for sympathetic innervation. All ventricular innervation was included, epicardial and intramyocardial. The label data was used to generate volume information for the myocardium of the ventricle and innervation. To measure the coronary vessels, similar volume measurements were performed for the lumen of the coronary vasculature. Measurements were performed blind and no animals were excluded. For controls we used Cre-negative hetero- and homozygous floxed littermates as well as Cre-positive mice that had not inherited floxed alleles.

Immunohistochemistry-whole mount staining

Mouse hearts were prepared and fixed as described above and subsequently dehydrated by methanol series (50-100%) and bleached overnight in 6% H_2O_2 in methanol. Hearts were then re-hydrated, blocked in PBSGT blocking buffet (0.2% gelatin (Sigma, G7041), 0.5% Triton X-100 (Merck, T8787) and 0.01% thimerosal in PBS) for 2-4 days. Primary antibodies were diluted in PBSGT as follows: goat polyclonal anti-cardiac Troponin I (cTnI, 1:200; Hytest Ltd, 4T21/2), rabbit polyclonal anti-Tyrosine Hydroxylase (TH, 1:200; Millipore, AB152). Hearts were incubated in primary antibodies at 37°C for 1 week. Afterwards, the hearts were washed six times with PBSGT at room temperature before secondary antibody incubation in PBSGT for 2 days. Subsequently, the hearts were washed six times for 1 hour in PBSGT. The hearts were then dehydrated in a graded tetrahydroflurane (THF, Sigma-Aldrich, 186562) series (50%, 80%, and 100%) and delipidated in dichloromethane (DCM, Sigma-Aldrich, D65100). Finally, samples were incubated in dibenzyl ether (DBE, Sigma-Aldrich, 108014) until clear and stored in DBE at room temperature. Samples were imaged on a light-sheet microscope (Zeiss, lightsheet Z.1). 3D-rendered images were visualized and captured with Imaris software (Bitplane, Version 7.6.4).

Explant co-cultures

Ventricles and stellate ganglia (STG) were dissected out from E14.5 or E15.5 mouse embryos with the indicated genotype, placed in PBS and cut into pieces and plated into a three-dimensional collagen matrix (3D collagen cell culture system, Chemicon) concurrently in DMEM media containing 15% fetal bovine serum (FBS, Sigma, F7524) for three days. The ventricle was placed 300-500μm away from the STG. Myocardium and neurite outgrowth were visualised by immunostaining whole-mount explants with rabbit polyclonal anti-

Peripherin (1:200; Millipore, AB1530) and goat polyclonal anti-cardiac Troponin I (cTnI, 1:200; Hytest Ltd, 4T21/2), followed by immunofluorescence detection using Alexa Fluor secondary antibodies. For quantitative analysis of the extent of axon growth from the STG into the heart, fluorescence images were captured at 4μm steps by using a spinning disk confocal microscope (PE Ultraview spinning disk). These pictures were projected over the Z axis and then merged manually using Volocity software (Quorum Technologies Inc.). STG explants were divided into forward and backward portions from the centre. The axons growing toward the ventricles were measured using 3D reconstruction software (Amira 6.3.0, Thermo Fisher Scientific).

Electrocardiography (ECG) studies

ECG recording of heart rate (HR) was acquired with MouseMonitor software (INDUS instruments). 2-3 months old male mice were anaesthetized with 1.5% isoflurane (IsoFlo Zoetis) in oxygen and kept at a constant 37° temperature using a heating pad for the duration of analysis. Following baseline reading, mice were challenged by isoproterenol (Acros, 14190250, 0.5 mg/kg by intraperitoneal injection).

Statistics

Detailed statistics and p-values are indicated in the figure legends. T-test or one-way ANOVA with Tukey's Test have been applied as indicated. Minimum to maximum box-violin plots are shown with all data points.

Results

Constitutive knock-out analysis indicates a role for Slit2 and Robo1 during cardiac innervation development

To test if Slit-Robo signalling is important for cardiac innervation guidance, we first analysed constitutive mouse knock-outs for ventricular innervation at embryonic day (E)14.5/E15.5 and E18.5 using Peripherin to label the total innervation (Figure 1A-B). *Slit1*$^{-/-}$ hearts did not show a phenotype at E14.5, but *Slit2*$^{-/-}$ hearts showed significantly reduced ventricular innervation. While *Slit3*$^{-/-}$ hearts showed increased levels of innervation compared to wild-type littermate controls at E14.5, this difference was not significant anymore at E18.5. Whereas the innervation was not affected in *Robo2*$^{-/-}$ mutants, the phenotype seen in *Slit2*$^{-/-}$ hearts was recapitulated in *Robo1*$^{-/-}$ hearts at E14.5 and still present at E18.5. Simultaneously knocking out *Robo1* and *Robo2* did not further increase the defects seen in the single *Robo1*$^{-/-}$ hearts at E15.5. We confirmed that these results were not influenced by differences in ventricular volume between the mutants and wild-type controls (Figure 1C). This data indicates a role for Slit2 and Robo1 during cardiac innervation development.

The coronary endothelium acts as a source of chemo-attractive Slit2 that guides the Robo1-positive nerves during heart development

Previously we have shown expression of the different Slit ligands and Robo receptors in cell-types such as the myocardium, endocardium and cushions/valves and their involvement in congenital heart disease.[22–24] As cardiac innervation follows the developing coronary vasculature,[4,17] here, we specifically focused on expression of the genes in the ventricular innervation and coronaries (Figure 2A). Immunohistochemistry at E18.5 found Slit2 ligand in the endothelium of the coronary veins and arteries, but not in the nerves extending into the

heart. At E14.5, Slit3 was neither present in the vessels nor innervation (data not shown), but at E18.5, Slit3 was highly present in the coronary smooth muscle wall and in the larger epicardial nerves, and minimally in intra-myocardial nerves. Both the Robo1 and Robo2 receptors were present in the nerves and at low levels in the arteries. Together with the knock-out data, this suggests that the coronary endothelium could act as source of chemo-attractive Slit2 that guides the Robo1-positive nerves during heart development.

Therefore, we further focused on the role of Slit2 and knocked-out *Slit2* specifically in the endothelium, which recapitulated the defects seen in the constitutive *Slit2*$^{-/-}$ hearts (Figure 2B), which were still visible at E18.5. As Slit2 is also highly expressed in trabecular myocardium, which could act as long-range guidance cue, we additionally removed *Slit2* specifically from the myocardium, which did not show a phenotype compared to wild-type controls at E18.5. While the constitutive double *Robo1/2* knockout did not show an additional role for Robo2 over Robo1 (Figure 1B), this could be caused by Robo2 being expressed in both the endothelium and innervation resulting in opposing signals. We hence deleted *Robo2* in the innervation and endothelium of constitutive *Robo1*$^{-/-}$ mice. *Robo1*$^{-/-}$ hearts showed the same reduction in innervation compared to wild-types as before, which was again not enhanced by specific removal of *Robo2* from the innervation or endothelium (Figure 2B).

Reduced sympathetic innervation in absence of endothelial Slit2 limits sympathetic stimulation of heart rate

To characterize the type of innervation affected in the endothelial Slit2 knock-out, we specifically quantified sympathetic innervation, which recapitulated the defects seen in the total innervation analysis (Figure 3A-B), showing that endothelial Slit2 guides the sympathetic innervation during heart development. To ensure that endothelial knock-out of Slit2 does not affect coronary vessel formation, we also quantified coronary vessel volumes,

showing no difference to controls (Figure 3C-D). Additionally, we validated the specificity of *Slit2* knock-out. Endothelial mutants showed absence of Slit2 from the endothelial cells, however, endocardial expression surrounding the trabeculae was still present (Figure 3E). This is likely caused by secretion of Slit2 from the strongly Slit2 positive trabecular myocardium.[23,24] To further confirm the chemo-attractive role of endothelial Slit2, we cultured wild-type stellate ganglia on their own or in presence of wild-type or endothelial *Slit2* knock-out ventricles. Attraction of axons extending from the ganglia was strongly reduced in the absence of endothelial Slit2 compared to wild-type ventricles (Figure 3F-G). Finally, to confirm functional relevance, we compared heart rate in adult endothelial Slit2 mutants and controls. While baseline heart rates were similar, Slit2 knock-out reduced heart rate increase after sympathetic stimulation with isoproterenol (Figure 3H-I). Combined, this data shows that endothelial Slit2 guides sympathetic innervation during heart development and absence results in functional defects.

Discussion

We have identified an important new chemo-attractive pathway mediated by Slit2 which is required for correct cardiac innervation development. This is somewhat unexpected as Slit2 is mainly known as a chemo-repulsive ligand, repelling extending axons.[28] However, many chemo-active ligands are bifunctional and can promote as well as inhibit axon growth, depending on the circumstances.[36–38] In case of Slit2, it has been shown that cleavage of the ligand and concentration levels are important for its bifunctionality. [39–41] Additionally, the specific chemo-active function of Slit2 can further be modulated by the type of extracellular matrix present.[41] How the attractive function of Slit2 in axon guidance during heart development is regulated will need to be determined.

The increase in innervation in constitutive *Slit3*$^{-/-}$ hearts at E14.5 could suggest that Slit3 has a chemo-repulsive role during early innervation development. However, this effect was not visible anymore around birth and could be caused by the nerves following the abnormal caval vein connections to the heart that are present in this mutant.[24] An indirect effect on innervation is supported by the limited expression of Slit3 in relevant cell-types at E14.5. After E14.5, multiple cell-types start to express Slit3 and the gene also becomes expressed in the large innervation, indicating expression is only turned on as the axons mature. The Slit-Robo pathway is best known for its role during nervous system development, where commissural neurons only become sensitive to repulsive Slit after midline crossing to prevent them from recrossing.[42] A similar temporal activation of the different genes of the pathway in the different cell-types would allow for complex control over where and when axons develop, which will need further investigation. While our data indicates that the innervation responds to endothelial Slit2 through the Robo1 receptor, we also find Robo1 expressed in the endothelium itself. This needs further examination using a conditional Robo1 line, which we failed to generate successfully.[22] These complicated spatio-temporal expression patterns of the genes of the Slit-Robo pathway could be key for determining the sympathetic versus parasympathetic balance or the patterning along veins and arteries.[17,35] Thus, our discovery of an important role for the Slit-Robo signalling pathway during cardiac innervation development raises new exiting questions that will need further investigation.

Acknowledgements

Sources of Funding

This work was supported by the British Heart Foundation (PG/15/50/31594), EMBO (ALTF 441-2010), Netherlands Organisation for Scientific Research (825.10.025) and European

Research Council (ERC) (715895, CAVEHEART) to MTMM, Oxford BHF Centre of Research Excellence by grant code (RE/18/3/34214) to SB, UKRI-MRC (MR/W006731/1) to KL, BHF FS/19/31/34158 to JV and BBSRC BB/W015277/1 to JV and MTMM.

Disclosures

None

References

1. Mangoni, M. E. & Nargeot, J. Genesis and regulation of the heart automaticity. *Physiol Rev* **88**, 919–982 (2008).
2. Ieda, M. & Fukuda, K. Cardiac innervation and sudden cardiac death. *Curr Cardiol Rev* **5**, 289–295 (2009).
3. Crick, S. J. *et al.* Innervation of the human cardiac conduction system. A quantitative immunohistochemical and histochemical study. *Circulation* **89**, 1697–1708 (1994).
4. Salamon, R. J. *et al.* Parasympathetic and sympathetic axons are bundled in the cardiac ventricles and undergo physiological reinnervation during heart regeneration. *iScience* **26**, 107709 (2023).
5. Wagner, J. U. G. *et al.* Aging impairs the neurovascular interface in the heart. *Science (1979)* **381**, 897–906 (2023).
6. Kapa, S., Venkatachalam, K. L. & Asirvatham, S. J. The autonomic nervous system in cardiac electrophysiology: an elegant interaction and emerging concepts. *Cardiol Rev* **18**, 275–284 (2010).
7. Chen, P. S. *et al.* Sympathetic nerve sprouting, electrical remodeling and the mechanisms of sudden cardiac death. *Cardiovasc Res* **50**, 409–416 (2001).
8. Chen, P. S., Chen, L. S., Fishbein, M. C., Lin, S. F. & Nattel, S. Role of the autonomic nervous system in atrial fibrillation: Pathophysiology and therapy. *Circ Res* **114**, 1500–1515 (2014).
9. Florea, V. G. & Cohn, J. N. The autonomic nervous system and heart failure. *Circ Res* **114**, 1815–1826 (2014).
10. Gardner, R. T. *et al.* Targeting protein tyrosine phosphatase σ after myocardial infarction restores cardiac sympathetic innervation and prevents arrhythmias. *Nat Commun* **6**, 6235 (2015).
11. Vaseghi, M., Lux, R. L., Mahajan, A. & Shivkumar, K. Sympathetic stimulation increases dispersion of repolarization in humans with myocardial infarction. *Am J Physiol Heart Circ Physiol* **302**, H1838-46 (2012).
12. Miwa, K. *et al.* Axon guidance of sympathetic neurons to cardiomyocytes by glial cell line-derived neurotrophic factor (GDNF). *PLoS One* **8**, e65202 (2013).
13. Kimura, K., Ieda, M. & Fukuda, K. Development, maturation, and transdifferentiation of cardiac sympathetic nerves. *Circ Res* **110**, 325–336 (2012).
14. Maden, C. H. *et al.* NRP1 and NRP2 cooperate to regulate gangliogenesis, axon guidance and target innervation in the sympathetic nervous system. *Dev Biol* **369**, 277–285 (2012).
15. Ieda, M. *et al.* Nerve growth factor is critical for cardiac sensory innervation and rescues neuropathy in diabetic hearts. *Circulation* **114**, 2351–2363 (2006).
16. Kuruvilla, R. *et al.* A neurotrophin signaling cascade coordinates sympathetic neuron development through differential control of TrkA trafficking and retrograde signaling. *Cell* **118**, 243–255 (2004).
17. Poltavski, D. M. *et al.* Venous endothelin modulates responsiveness of cardiac sympathetic axons to arterial semaphorin. *Elife* **8**, 1–23 (2019).
18. Ieda, M. *et al.* Sema3a maintains normal heart rhythm through sympathetic innervation patterning. *Nat Med* **13**, 604–612 (2007).
19. Blockus, H. & Chédotal, A. Slit-Robo signaling. *Development* **143**, 3037–3044 (2016).

361 20. Jiang, Z. *et al.* Targeting the SLIT/ROBO pathway in tumor progression: molecular
362 mechanisms and therapeutic perspectives. *Therapeutic Advances in Medical*
363 *Oncology* vol. 11 Preprint at https://doi.org/10.1177/1758835919855238 (2019).
364 21. Zhao, J. & Mommersteeg, M. T. M. Slit-Robo signalling in heart development.
365 *Cardiovasc Res* **cvy061**, (2018).
366 22. Zhao, J., Bruche, S., Potts, H. G., Davies, B. & Mommersteeg, M. T. M. Tissue-Specific
367 Roles for the Slit–Robo Pathway During Heart, Caval Vein, and Diaphragm
368 Development. *J Am Heart Assoc* **11**, (2022).
369 23. Mommersteeg, M. T. M., Yeh, M. L., Parnavelas, J. G. & Andrews, W. D. Disrupted Slit-
370 Robo signalling results in membranous ventricular septum defects and bicuspid aortic
371 valves. *Cardiovasc Res* **106**, 55–66 (2015).
372 24. Mommersteeg, M. T. M. *et al.* Slit-roundabout signaling regulates the development of
373 the cardiac systemic venous return and pericardium. *Circ Res* **112**, 465–475 (2013).
374 25. Andrews, W. *et al.* The role of Slit-Robo signaling in the generation, migration and
375 morphological differentiation of cortical interneurons. *Dev Biol* **313**, 648–658 (2008).
376 26. Lu, W. *et al.* Disruption of ROBO2 is associated with urinary tract anomalies and
377 confers risk of vesicoureteral reflux. *Am J Hum Genet* **80**, 616–632 (2007).
378 27. Rama, N. *et al.* Slit2 signaling through Robo1 and Robo2 is required for retinal
379 neovascularization. *Nat Med* **21**, 483–491 (2015).
380 28. Plump, A. S. *et al.* Slit1 and Slit2 cooperate to prevent premature midline crossing of
381 retinal axons in the mouse visual system. *Neuron* **33**, 219–232 (2002).
382 29. Gibson, D. A. *et al.* Dendrite self-avoidance requires cell-autonomous slit/robo
383 signaling in cerebellar purkinje cells. *Neuron* **81**, 1040–1056 (2014).
384 30. Yuan, W. *et al.* A genetic model for a central (septum transversum) congenital
385 diaphragmatic hernia in mice lacking Slit3. *Proc Natl Acad Sci U S A* **100**, 5217–5222
386 (2003).
387 31. Danielian, P. S., Muccino, D., Rowitch, D. H., Michael, S. K. & McMahon, A. P.
388 Modification of gene activity in mouse embryos in utero by a tamoxifen-inducible
389 form of Cre recombinase. *Curr Biol* **8**, 1323–1326 (1998).
390 32. Koni, P. A. *et al.* Conditional vascular cell adhesion molecule 1 deletion in mice:
391 Impaired lymphocyte migration to bone marrow. *Journal of Experimental Medicine*
392 **193**, 741–753 (2001).
393 33. Sohal, D. S. *et al.* Temporally regulated and tissue-specific gene manipulations in the
394 adult and embryonic heart using a tamoxifen-inducible Cre protein. *Circ Res* **89**, 20–
395 25 (2001).
396 34. Mommersteeg, M. T. M. *et al.* The sinus venosus progenitors separate and diversify
397 from the first and second heart fields early in development. *Cardiovasc Res* (2010)
398 doi:10.1093/cvr/cvq033.
399 35. Schneider, C. a, Rasband, W. S. & Eliceiri, K. W. NIH Image to ImageJ: 25 years of
400 image analysis. *Nat Methods* **9**, 671–675 (2012).
401 36. Wong, J. T. W., Wong, S. T. M. & O'Connor, T. P. Ectopic semaphorin-1a functions as
402 an attractive guidance cue for developing peripheral neurons. *Nat Neurosci* **2**, (1999).
403 37. De Castro, F., Hu, L., Drabkin, H., Sotelo, C. & Ché Dotal, A. *Chemoattraction and*
404 *Chemorepulsion of Olfactory Bulb Axons by Different Secreted Semaphorins*. (1999).
405 38. Colamarino, S. A. & Tessier-Lavigne, M. *The Axonal Chemoattractant Netrin-I Is Also a*
406 *Chemorepellent for Trochlear Motor Axons*. *Cell* vol. 81 (1995).

39. Pilling, D., Chinea, L. E., Consalvo, K. M. & Gomer, R. H. Different Isoforms of the Neuronal Guidance Molecule Slit2 Directly Cause Chemoattraction or Chemorepulsion of Human Neutrophils. *The Journal of Immunology* **202**, 239–248 (2019).
40. Bhosle, V. K. *et al.* The chemorepellent, SLIT2, bolsters innate immunity against Staphylococcus aureus. *Elife* **12**, (2023).
41. Nguyen-Ba-Charvet, K. T. *et al.* Sensory axon response to substrate-bound Slit2 is modulated by laminin and cyclic GMP. *Molecular and Cellular Neuroscience* **17**, 1048–1058 (2001).
42. Bisiak, F. & McCarthy, A. A. Structure and Function of Roundabout Receptors. in *Macromolecular Protein Complexes II: Structure and Function* 291–319 (2020). doi:10.1007/978-3-030-28151-9_9.

Figures and Figure Legends

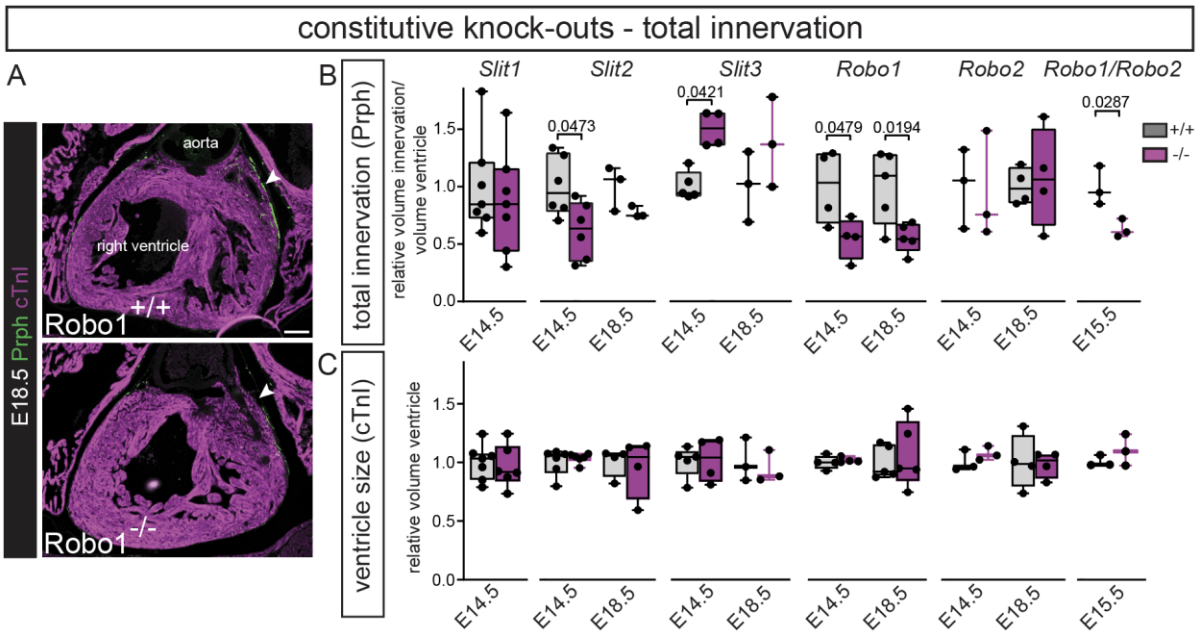

Figure 1. Constitutive knock-out analysis indicates a role for Slit2, Slit3 and Robo1 during cardiac innervation development. A, Representative images of *Robo1*$^{+/+}$ and *Robo1*$^{-/-}$ sections stained by immunohistochemistry for the myocardium using cardiac Troponin I (cTnI) in purple and total innervation using Peripherin (Prph) in green. Arrowhead points to reduced total innervation staining in green in the *Robo1*$^{-/-}$. B, Quantification of total ventricular innervation corrected for ventricle volume (myocardial marker cTnI) in constitutive knock-outs and wild-type controls. T-test or one-way ANOVA with Tukey's Test per mouse line. C, Quantification of total ventricular volume based on myocardial marker cTnI in constitutive knock-outs and wild-type controls. T-test or one-way ANOVA with Tukey's Test per mouse line. Scale bar 100µm.

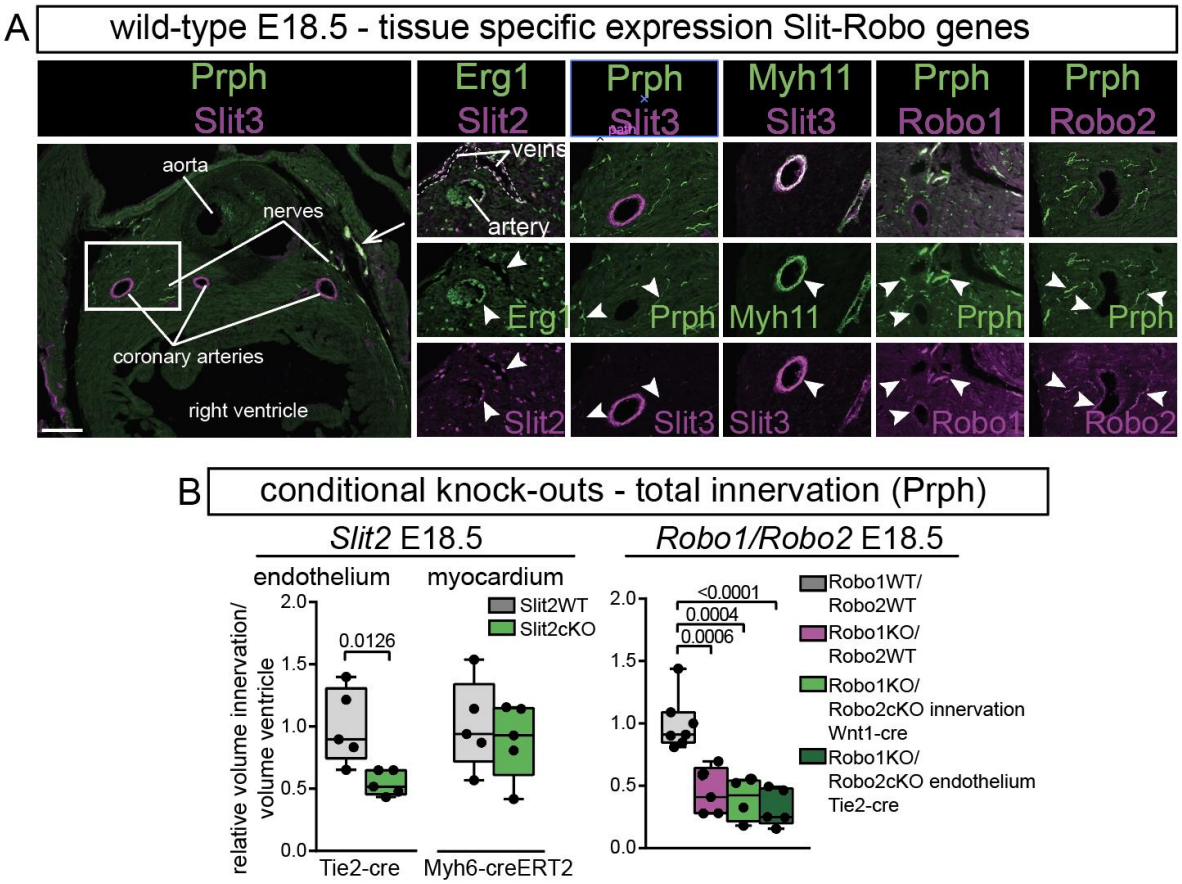

Figure 2. The coronary endothelium acts as source of chemo-attractive Slit2 that guides the Robo1-positive nerves during heart development. A, Immunohistochemistry for Slit2, Slit3, Robo1, Robo2, endothelial marker Erg1, innervation marker Prph and smooth muscle marker Myh11 at E18.5. Box indicates region of magnification. Arrow points to overlap Slit3 and Prph in the large epicardial nerves. White arrowheads point to region of absence or presence of co-localisation of the indicated genes. B. Measurements of total ventricular innervation corrected for ventricle volume in the indicated conditional knock-outs and wild-type controls. T-test or one-way ANOVA with Tukey's Test. Scale bar 100µm.

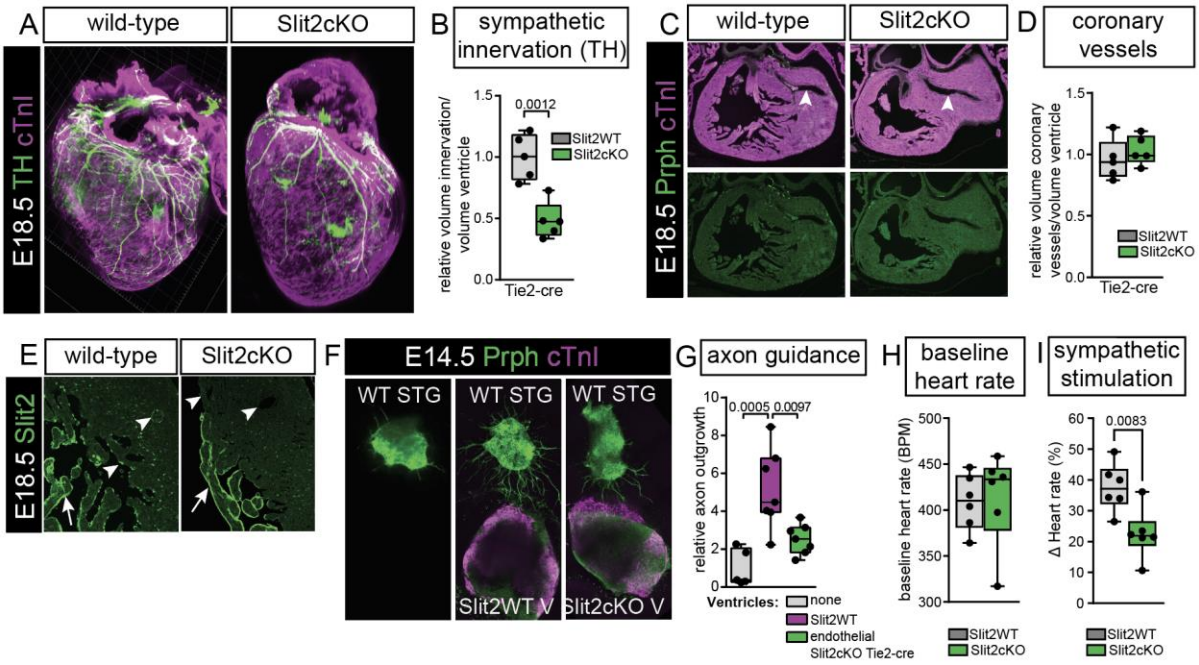

Figure 3. Reduced sympathetic innervation in absence of endothelial Slit2 limits sympathetic stimulation of heart rate. A, Immunohistochemistry for sympathetic innervation marker TH and myocardial marker cTnI on whole mount E18.5 hearts. B, Quantification of sympathetic innervation corrected for ventricle volume in endothelial Slit2 knock-outs versus controls. T-test. C, Immunohistochemistry for total innervation marker Prph and myocardial marker cTnI on E18.5 sections. Arrowheads point to the normal development of the coronary vessels. D, Quantification of coronary vessel volume corrected for ventricle volume in endothelial Slit2 knock-outs versus controls. T-test. E, Immunohistochemistry for Slit2 on endothelial Slit2 knock-outs versus controls, showing the lack of Slit2 in the endothelium. F, E14.5 ventricles and stellate ganglia (STG) cultured in three-dimensional collagen matrix (Chemicon) for 3 days. Immunohistochemistry for Prph and cTnI. G, Quantification of axon outgrowth. One-way ANOVA with Tukey's Test. H, Quantification of baseline heart rate using electrocardiogram. G, Quantification of heart rate after stimulations with isoproterenol. Scale bar 100μm.